SUPPORTING INFORMATION

SMM behavior tuned by an exchange coupling LEGO® approach for chimeric compounds: First 2p-3d-4f hetero-tri-spin complexes with different metal ions bridged by one aminoxyl group

Andrei A. Patrascu,[†] Matteo Briganti,[‡,#] Stéphane Soriano,[¶] Sergiu Calancea,[†,&] Rafael A. Allão Cassaro,[§] Federico Totti*[,‡], Maria G. F. Vaz*[,#], Marius Andruh*[,†]

[†] *Inorganic Chemistry Laboratory, Faculty of Chemistry, University of Bucharest, Str. Dumbrava Rosie nr. 23, 020464-Bucharest, Romania*

[‡]*Department of Chemistry "Ugo Schiff" and INSTM RU University of Florence, 50019 Sesto Fiorentino, Italy.*

[¶] *Universidade Federal Fluminense, Instituto de Física, 24210-346-Niterói, Rio de Janeiro, Brazil*

[&] *Moldova State University, MD-2009-Chisinau, Faculty of Chemistry and Chemical Technology, Moldova*

[§] *Instituto de Química, Universidade Federal do Rio de Janeiro,* 21941-909-*Rio de Janeiro, Brazil*

[#] *Universidade Federal Fluminense, Instituto de Química, 24020-346-Niterói, Rio de Janeiro, Brazil*

SYNTHESES

The Mannich base was synthesized following the procedure published by Fenton *et al*.[1] The typical procedure for the synthesis of ligands and the corresponding complexes is illustrated below.

Synthesis of the chiral Mannich Base *R*-/*S*- (Scheme S1)

(*R*)-(+)-*N*,α-Dimethylbenzylamine (0.5680 g, 4.2 mmoles), paraformaldehyde (0.2180 g, 7.2 mmoles) and 5-bromosalicylaldehyde (1 g, 4.97 mmoles) were refluxed in 50 mL methanol for five days. The yellow solution was cooled and the solvent was evaporated under reduced pressure, affording a yellow sticky oil. The chiral Mannich base was purified on a SiO_2 chromatography column. The unreacted 5-bromosalicylaldehyde was eliminated using dicholoromethane, while the main product was eluated with ethyl acetate [0.8090 g; . yield: 47 %

(*R*); 0.5320 g; yield: 31% (*S*)]. FTIR (cm^{-1}): 2975 (w), 1596 (w), 1450 (s), 1364 (vs), 1223 (m), 1135 (m), 1029 (m), 862 (m), 738 (m), 701 (s), 667 (w), 542 (m), 454 (m).

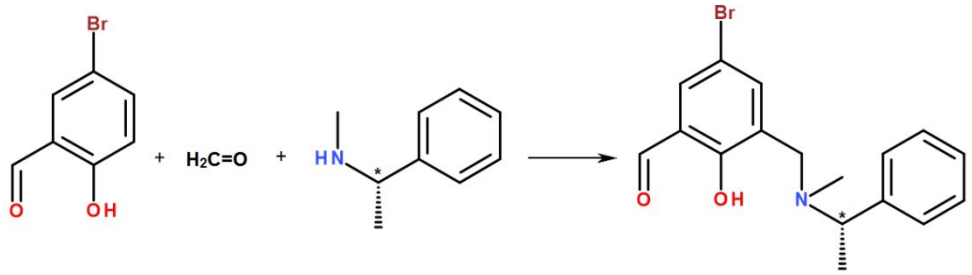

Scheme S1. Synthesis of the chiral Mannich base.

Synthesis of the chiral nitronyl-nitroxide *R*-/*S*-HL[4] (Scheme S2)

To a methanolic solution (40 mL) of [2,3-bis(hydroxyamino)-2,3-dimethylbutane]·H_2SO_4 (0. 0.3925 g, 1.59 mmoles), which was deprotonated with 0.7 mL Et_3N, the (*R*-/*S*-) Mannich base (0. 0.5546 g, 1.59 mmoles) was added under stirring at room temperature. The resulting mixture was stirred at room temperature for four days, then concentrated under reduced pressure giving the reaction product as a pale-yellow oil which was solubilized in 50 ml dichloromethane. To the resulted solution solid KIO_4 was added, then 20 mL water. The mixture was vigorously stirred for one hour at 0° C, then dried over anhydrous $MgSO_4$ and concentrated under reduced pressure to obtain a purple oil. The stable nitronyl nitroxide radical was purified on a chromatography column (SiO_2) using diethyl ether as eluent. The organic solution was dried over anhydrous magnesium sulfate and concentrated under reduced pressure to obtain a purple solid [0.2460 g, yield: 46 % (*R*); 0.3180 g yield: 59% (*S*)]. FTIR KBr pellet (cm^{-1}): 3402 (w), 2962 (w), 2934 (w), 1656 (m), 1594 (w),1453 (vs), 1403 (s), 1367 (vs), 1336 (s), 1297 (m), 1259 (m), 1207 (s), 1164 (s), 1136 (w), 1092 (w), 1053 (w), 864 (w), 756 (m), 703 (m), 663 (w), 543 (w), 455 (w).

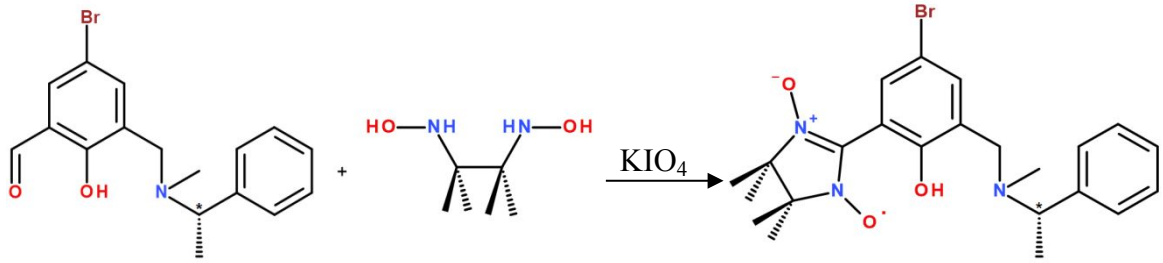

Scheme S2. Synthesis of the chiral nitronyl-nitroxide ligands.

Synthesis of [CoDy(hfac)$_5$(*R*-HL^4)]. To 20 mL hot *n*-heptane solution of [Co(hfac)$_2$(H$_2$O)$_2$] (0.016 g, 0.031 mmol) and [Dy(hfac)$_3$(H$_2$O)$_3$] (0.026 g, 0.031 mmol), a chloroform solution (2 mL) of *R*-HL^4 (0.015g, 0.031 mmol) was added and the mixture was stirred for one minute. The resulting solution was cooled down to room temperature and purple crystals were obtained after few hours. FTIR (cm^{-1}): 1643 (m), 1531 (m), 1503 (m), 1453 (m), 1345 (w), 1252 (s), 1195 (s), 1139 (vs), 1096 (s), 950 (w), 797 (m), 660 (s), 585 (m), 527 (w), 457 (w), 417 (w).

Synthesis of the nitronyl-nitroxide from 5-bromosalicylaldehyde, *HL*. The synthesis of HL radical have been performed in similar way as for *R*-/*S*-HL^4 nitroxides, using 2 mmoles of [2,3-bis(hydroxyamino)-2,3-dimethylbutane]·H$_2$SO$_4$ and 5-bromosalicylaldehyde**,** (0.260 g, yield: 40 %).

Synthesis of (HNEt$_3$)[DyL(hfac)$_3$] 12. To 20 mL hot *n*-heptane solution of [Dy(hfac)$_3$(H$_2$O)$_2$] (0.026 g, 0.03 mmol), a chloroform solution (2 mL) of HL (0.010 g, 0.03 mmol) containing two drops of triethylamine, was added and the mixture was stirred for one minute. The resulting solution was cooled down to room temperature and blue-purple crystals were obtained after three days, (0.028 g, yield: 77 %).

Synthesis of (HNEt$_3$)$_2$[CoL(hfac)$_2$][Tb(hfac)$_4$] 13. To 20 mL hot *n*-heptane solution of [Co(hfac)$_2$(H$_2$O)$_2$] (0.016 g, 0.03 mmol) and [Tb(hfac)$_3$(H$_2$O)$_3$] (0.026 g, 0.03 mmol), a chloroform solution (2 mL) of HL (0.010 g, 0.03 mmol) containing two drops of triethylamine, was added and the mixture was stirred for one minute. The solution was then allowed to cool to room temperature. After three days a blue-purple crystals were obtained, (0.030 g, yield: 58 %).

Physical Measurements.

IR spectra (KBr pellets) were recorded on a Tensor 37 spectrophotometer in the 4000-400 cm^{-1} region. Diffused reflectance circular dichroism (DRCD) spectra of crystalline samples were performed on a JASCO J-1500 spectrophotometer equipped with an integrating sphere attachment (DRCD-575 accessory) in the 200-800 nm domain at a scan rate of 100 nm/min and accumulated twelve times. DC magnetic measurements were carried out using a Quantum

Design MPMS SQUID magnetometer. All compounds were wrapped in polytetrafluoroethylene (PTFE) tape and pressed into a pellet before measurement. Magnetic data were corrected for the sample holder and diamagnetic contributions for all magnetic measurements. AC magnetic measurements were performed on a Quantum Design PPMS using the ACMS option. Powder X-Ray Diffraction patterns have been recorded with a Bruker D8 Advance diffractometer (CuKα radiation).

Crystallographic Data Collection and Structure Determination.

X-ray diffraction measurements were performed on a STOE IPDS II and on a Bruker D8 Venture diffractometers operating with a Mo Kα (λ = 0.71073 Å) X-ray tube with graphite X monochromator The structures were solved (SHELXS-2014) by direct methods and refined (SHELXL-2014)by full matrix least-squares procedures on F^2.[2] All non-H atoms of the donor molecules were refined anisotropically, and hydrogen atoms were introduced at calculated positions (riding model), included in structure factor calculations, but not refined. Due to large conformational disorder and to thermal motion present in CF3, large thermal displacement parameters were found for disordered fluorine atoms. Crystals of compound **13** have poor quality and are weakly diffracting. Crystallographic data for the structures have been deposited in the Cambridge Crystallographic Data Centre, deposition numbers CCDC 1922779-1922792. These data can be obtained free of charge from the Cambridge Crystallographic Data Centre via www.ccdc.cam.ac.uk/data_request/cif

Table S1. Crystallographic data, details of data collection and structure refinement parameters for compounds **1 - 13**.

Compound	[CoDy(L^1H)(hfac)$_5$] **1**	[CoGd(L^2H)(hfac)$_5$] **2**	[CoGd(L^3H)(hfac)$_5$] **3**	[MnGd(L^3H)(hfac)$_5$] **4**
Formula	$C_{45}H_{25}N_3O_{13}F_{30}BrCoDy$	$C_{47}H_{32}N_3O_{13}F_{30}BrCoGd$	$C_{53}H_{36}N_3O_{13}F_{30}BrCoGd$	$C_{53}H_{36}N_3O_{13}F_{30}BrMnGd$
Formula weight/ g mol^{-1}	1687.02	1712.84	1788.94	1784.95
T/K	293(2)	293(2)	298(2)	298(2)
λ/Å	0.71073	0.71073	0.71073	0.71073
Crystal system	Triclinic	Triclinic	Monoclinic	Monoclinic
Space group	P-1	P-1	C2/c	C2/c
Unit cell				
a/Å	12.729(2)	13.5135(13)	24.183(5)	24.210(5)
b/Å	14.0138(18)	13.8747(13)	13.543(3)	13.574(3)
c/Å	19.107(3)	19.3461(19)	40.886(8)	41.013(8)
α/deg	69.490(11)	92.128(8)	90	90
β/deg	88.593(13)	103.288(8)	90.41(3)	90.06(3)
γ/deg	85.933(12)	117.14(7)	90	90
V/Å^3	3184.3(9)	3098.8(18)	13391(5)	13478(5)
Z	2	2	8	8
Calculated density/g cm−3	1.772	1.836	1.775	1.759
Absorption coefficient/cm−1	2.197	2.123	1.970	1.898
F(000)	1660	1670	7000	6984
Crystal size/mm × mm × mm	0.3 x 0.15 x 0.04	0.2 x 0.3 x 0.3	0.2 x 0.2 x 0.3	0.2 x 0.2 x 0.3
θ range/deg	1.966 to 25.000	1.757 to 24.998	1.684 to 25.000	1.682 to 25.000
Limiting indices	-14 < h < 15, -16 < k < 16 -22 < l < 22	-16 < h < 16, -16 < k < 16 -22 < l < 22	-28 < h < 28, -16 < k < 16 -48 < l < 48	-28 < h < 28, -16 < k < 16 -47 < l < 48
Collected reflections	28240	31218	27947	58120
Symmetry independent reflections	11135	10792	11217	11843
R_{int}	0.1410	0.1221	0.1089	0.0572
Data/restraints/ parameters	11135 / 101 / 822	10792 / 33 / 875	11217 / 31 / 910	11843 / 6 / 916
GOF on F^2	1.156	1.047	0.997	1.012
Final R indices	R1 = 0.1094 wR2 = 0.1893	R1 = 0.0701 wR2 = 0.1565	R1 = 0.0803 wR2 = 0.2122	R1 = 0.0659 wR2 = 0.1855
Largest diff peak and hole/e Å^{-3}	1.073 and -1.136	1.059 and -0.668	0.908 and -1.194	0.702 and -1.232

Compound	[CoDy(*R*-L^{4}H)(hfac)$_5$] **5a**	[CoDy(*S*-L^{4}H)(hfac)$_5$] **5b**	[CoGd(*R*-L^{4}H)(hfac)$_5$] **6**	[CoTb(*S*-L^{4}H)(hfac)$_5$] **7**
Formula	$C_{51.50}H_{42}N_3O_{13}F_{30}BrCoDy$	$C_{51.50}H_{42}N_3O_{13}F_{30}BrCoDy$	$C_{51.50}H_{42}N_3O_{13}F_{30}BrCoGd$	$C_{51.50}H_{42}N_3O_{13}F_{30}BrCoTb$
Formula weight/ g mol^{-1}	1782.22	1782.22	1776.97	1778.64
T/K	153(2)	153(2)	153(2)	150(2)
λ/Å	0.71073	0.71073	0.71073	0.71073
Crystal system	Triclinic	Triclinic	Triclinic	Triclinic
Space group	P1	P1	P1	P1
Unit cell				
a/Å	13.0196(5)	12.919(3)	13.0587(3)	12.879(3)
b/Å	14.3559(5)	14.117(3)	14.3543(4)	14.059(3)
c/Å	19.2553(7)	19.097(4)	19.2687(5)	19.103(4)
α/deg	110.187(2)	110.88(3)	110.399(2)	111.22(3)
β/deg	90.556(2)	90.84(3)	90.733(2)	90.71(3)
γ/deg	94.416(2)	93.72(3)	94.084(2)	93.52(3)
V/Å^3	3365.3(2)	3244.5(13)	3374.05(16)	3216.1(13)
Z	2	2	2	2
Calculated density/g cm−3	1.759	1.824	1.749	1.837
Absorption coefficient/cm−1	2.083	2.161	1.953	2.118
F(000)	1748	1748	1744	1746
Crystal size/mm × mm × mm	0.2 x 0.1 x 0.1	0.2 x 0.1 x 0.1	0.2 x 0.1 x 0.1	0.204 x 0.100 x 0.090
θ range/deg	1.968 to 26.446	1.913 to 32.056	1.892 to 32.016	2.143 to 26.526
Limiting indices	-16 < h < 16, -17 < k < 17 -24 < l < 24	-19 < h < 19, -20 < k < 20, -28 < l < 28	-19 < h < 19, -21 < k < 21, -28 < l < 28	-16 < h < 16, -17 < k < 17, -23 < l < 23
Collected reflections	259700	75437	221132	245032
Symmetry independent reflections	27546	39007	43945	26550
R_{int}	0.1631	0.1192	0.1584	0.0951
Data/restraints/ parameters	27546 / 95 / 1807	39007 / 80 / 1810	43945 / 63 / 1807	26550 / 38 / 1805
GOF on F^2	1.051	0.944	1.012	1.035
Final R indices	R1 = 0.0516 wR2 = 0.0918	R1 = 0.0664 wR2 = 0.1263	R1 = 0.0655 wR2 = 0.1142	R1 = 0.0376 wR2 = 0.0764
Largest diff peak and hole/e Å^{-3}	0.797 and -0.829	1.046 and -2.710	0.690 and -0.955	1.134 and -0.663

Compound	[ZnDy(*S*-L^{4}H)(hfac)$_5$] **8**	[NiDy(*S*-L^{4}H)(hfac)$_5$] **9**	[MnDy(*R*-L^{4}H)(hfac)$_5$] **10**	[Dy(L^{3}H)(hfac)$_3$] **11**
Formula	$C_{51.50}H_{42}N_3O_{13}F_{30}BrZnDy$	$C_{51.50}H_{42}N_3O_{13}F_{30}BrNiDy$	$C_{51.50}H_{42}N_3O_{13}F_{30}BrMnDy$	$C_{43}H_{34}N_3O_9F_{18}BrDy$
Formula weight/ g mol^{-1}	1788.66	1782.00	1778.23	1321.14
T/K	153(2)	298(2)	298(2)	298(2)
λ/Å	0.71073	0.71073	0.71073	0.71073
Crystal system	Triclinic	Triclinic	Triclinic	Monoclinic
Space group	P1	P1	P1	P21/c
Unit cell				
a/Å	12.9916(8)	13.0760(4)	12.913(3)	11.894(2)
b/Å	14.3968(10)	14.2401(4)	14.231(3)	30.290(6)
c/Å	19.2533(13)	19.2592(6)	19.189(4)	14.729(3)
α/deg	110.191(5)	110.599(2)	110.78(3)	90
β/deg	90.671(5)	91.084(2)	90.75(3)	105.48(3)
γ/deg	94.449(5)	93.584(3)	94.12(3)	90
V/Å^3	3366.8(4)	3347.07(18)	3285.5(13)	5114.2(19)
Z	2	2	2	4
Calculated density/g cm−3	1.764	1.768	1.797	1.716
Absorption coefficient/cm−1	2.192	2.128	2.074	2.362
F(000)	1754	1750	1744	2592
Crystal size/mm × mm × mm	0.3 x 0.4 x 0.4	0.2 x 0.1 x 0.1	0.2 x 0.1 x 0.1	0.3 x 0.3 x 0.3
θ range/deg	1.973 to 25.999	1.888 to 32.292	1.909 to 26.999	1.776 to 25.998
Limiting indices	-16 < h < 16, -17 < k < 17 -23 < l < 23	-19 < h < 19, -21 < k < 21 -28 < l < 28	-16 < h < 16, -18 < k < 18 -24 < l < 24	-14 < h < 14, -37 < k < 37 -18 < l < 18
Collected reflections	64537	138882	47588	59198
Symmetry independent reflections	24631	43309	27009	10025
R_{int}	0.1036	0.0729	0.0423	0.1361
Data/restraints/ parameters	24631 / 111 / 1810	43309 / 56 / 1810	27009 / 34 / 1810	10025 / 0 / 676
GOF on F^2	0.923	1.037	1.023	1.028
Final R indices	R1 = 0.0564 wR2 = 0.1174	R1 = 0.0650 wR2 = 0.1382	R1 = 0.0446 wR2 = 0.0993	R1 = 0.0575 wR2 = 0.1188
Largest diff peak and hole/e Å^{-3}	0.592 and -1.408	1.024 and -1.156	0.810 and -0.923	0.877 and -0.810

Compound	$(HNEt_3)[DyL(hfac)_3]$ **12**	$(HNEt_3)_2[CoL(hfac)_2][Tb(hfac)_4]$ **13**
Formula	$C_{34}H_{34}N_3O_9F_{18}BrDy$	$C_{55}H_{53}N_4O_{15}F_{36}BrCoTb$
Formula weight/ g mol^{-1}	1213.05	1991.77
T/K	298(2)	298(2)
λ/Å	0.71073	0.71073
Crystal system	Monoclinic	Monoclinic
Space group	P 21/c	P 21/n
Unit cell		
a/Å	12.427(3)	19.160(2)
b/Å	15.273(3)	19.3177(14)
c/Å	24.353(5)	21.095(2)
α/deg	90	90
β/deg	93.66(3)	108.454(8)
γ/deg	90	90
V/$Å^3$	4612.8(16)	7406.3(13)
Z	4	4
Calculated density/g cm−3	1.747	1.786
Absorption coefficient/cm−1	2.609	1.863
F(000)	2376	3928
Crystal size/mm × mm × mm	0.07 x 0.05 x 0.05	0.2 x 0.1 x 0.02
θ range/deg	2.115 to 26.000	2.031 to 22.722
Limiting indices	-14 < h < 15, -17 < k < 18 -30 < l < 30	-20 < h < 20, -20 < k < 20 -22 < l < 22
Collected reflections	21217	39792
Symmetry independent reflections	8608	9938
R_{int}	0.1423	0.2378
Data/restraints/ parameters	8608 / 0 / 593	9938/ 41 / 1015
GOF on F^2	1.000	1.049
Final R indices	R1 = 0.0608 wR2 = 0.1239	R1 = 0.1003 wR2 = 0.2024
Largest diff peak and hole/e $Å^{-3}$	0.792 and -0.966	0.921 and -1.005

Table S2. Selected bond distances (Å) and angles (°) for compounds **5a** and **5b**

[CoDy(*R*-L^{4}H)(hfac)$_5$] **5a**	[CoDy(*R*-L^{4}H)(hfac)$_5$] **5a**
N(1) - O(1) = 1.34(2)	O(1) - Co(1) - O(4) = 92.9(6)
N(2) - O(2) = 1.29(3)	O(1) - Co(1) - O(5) = 176.1(8)
Dy(1) - O(1) = 2.402(16)	O(1) - Co(1) - O(6) = 95.7(7)
Dy(1) - O(3) = 2.200(16)	O(1) - Co(1) - O(7) = 91.1(6)
Dy(1) - O(8) = 2.385(16)	O(1) - Co(1) - O(8) = 76.2(6)
Dy(1) - O(9) = 2.397(15)	O(4) - Co(1) - O(5) = 85.9(7)
Dy(1) - O(10) = 2.286(17)	O(4) - Co(1) - O(6) = 171.2(7)
Dy(1) - O(11) = 2.346(17)	O(4) - Co(1) - O(7) = 95.6(7)
Dy(1) - O(12) = 2.363(16)	O(4) - Co(1) - O(8) = 98.4(7)
Dy(1) - O(13) = 2.414(17)	O(5) - Co(1) - O(6) = 85.4(7)
Co(1) - O(1) = 2.101(16)	O(5) - Co(1) - O(7) = 92.7(8)
Co(1) - O(4) = 2.038(15)	O(5) - Co(1) - O(8) = 100.2(8)
Co(1) - O(5) = 2.013(19)	O(6) - Co(1) - O(7) = 86.1(7)
Co(1) - O(6) = 2.070(16)	O(6) - Co(1) - O(8) = 81.9(7)
Co(1) - O(7) = 2.055(19)	O(7) - Co(1) - O(8) = 161.5(7)
Co(1) - O(8) = 2.216(15)	O(1) - Dy(1) - O(3) = 74.7(5)
N(4) - O(14) = 1.34(2)	O(1) - Dy(1) - O(8) = 67.7(5)
N(5) - O(15) = 1.24(2)	O(1) - Dy(1) - O(9) = 113.7(5)
Dy(2) - O(14) = 2.386(16)	O(1) - Dy(1) - O(10) = 143.0(5)
Dy(2) - O(16) = 2.257(14)	O(1) - Dy(1) - O(11) = 78.8(5)
Dy(2) - O(17) = 2.406(19)	O(1) - Dy(1) - O(12) = 91.1(6)
Dy(2) - O(18) = 2.313(17)	O(1) - Dy(1) - O(13) = 144.7(5)
Dy(2) - O(19) = 2.376(15)	O(3) - Dy(1) - O(8) = 116.2(5)
Dy(2) - O(20) = 2.370(15)	O(3) - Dy(1) - O(9) = 80.2(5)
Dy(2) - O(21) = 2.219(18)	O(3) - Dy(1) - O(10) = 140.9(6)
Dy(2) - O(22) = 2.430(14)	O(3) - Dy(1) - O(11) = 145.4(6)
Co(2) - O(14) = 2.082(14)	O(3) - Dy(1) - O(12) = 87.8(6)
Co(2) - O(21) = 2.219(18)	O(3) - Dy(1) - O(13) = 74.7(6)
Co(2) - O(23) = 2.046(18)	O(8) - Dy(1) - O(9) = 71.0(5)
Co(2) - O(24) = 2.037(16)	O(8) - Dy(1) - O(10) = 82.8(5)
Co(2) - O(25) = 2.058(18)	O(8) - Dy(1) - O(11) = 71.9(5)
Co(2) - O(26) = 2.004(16)	O(8) - Dy(1) - O(12) = 140.0(5)
	O(8) - Dy(1) - O(13) = 143.7(5)
	O(9) - Dy(1) - O(10) = 74.3(6)
	O(9) - Dy(1) - O(11) = 131.5(5)
	O(9) - Dy(1) - O(12) = 148.1(6)
	O(9) - Dy(1) - O(13) = 77.6(6)
	O(10) - Dy(1) - O(11) = 71.0(6)
	O(10) - Dy(1) - O(12) = 98.5(6)
	O(10) - Dy(1) - O(13) = 71.3(6)
	O(11) - Dy(1) - O(12) = 70.9(6)
	O(11) - Dy(1) - O(13) = 120.0(6)
	O(12) - Dy(1) - O(13) = 70.7(6)
	O(14) - Co(2) - O(21) = 75.9(6)
	O(14) - Co(2) - O(23) = 93.7(7)
	O(14) - Co(2) - O(24) = 97.3(7)
	O(14) - Co(2) - O(25) = 175.3(8)
	O(14) - Co(2) - O(26) = 92.1(6)
	O(21) - Co(2) - O(23) = 165.6(7)
	O(21) - Co(2) - O(24) = 82.2(7)
	O(21) - Co(2) - O(25) = 99.3(7)
	O(21) - Co(2) - O(26) = 94.0(7)

O(23) - Co(2) - O(24) = 89.4(7)
O(23) - Co(2) - O(25) = 90.9(8)
O(23) - Co(2) - O(26) = 96.4(7)
O(24) - Co(2) - O(25) = 81.8(7)
O(24) - Co(2) - O(26) = 168.7(7)
O(25) - Co(2) - O(26) = 88.3(7)
O(14) - Dy(2) - O(16) = 74.2(5)
O(14) - Dy(2) - O(17) = 147.9(6)
O(14) - Dy(2) - O(18) = 91.7(6)
O(14) - Dy(2) - O(19) = 141.4(6)
O(14) - Dy(2) - O(20) = 78.0(6)
O(14) - Dy(2) - O(21) = 66.7(5)
O(14) - Dy(2) - O(22) = 114.2(6)
O(16) - Dy(2) - O(17) = 76.8(6)
O(16) - Dy(2) - O(18) = 85.0(6)
O(16) - Dy(2) - O(19) = 142.9(6)
O(16) - Dy(2) - O(20) = 142.9(6)
O(16) - Dy(2) - O(21) = 116.3(5)
O(16) - Dy(2) - O(22) = 80.7(6)
O(17) - Dy(2) - O(18) = 72.2(7)
O(17) - Dy(2) - O(19) = 70.2(7)
O(17) - Dy(2) - O(20) = 120.3(6)
O(17) - Dy(2) - O(21) = 140.9(6)
O(17) - Dy(2) - O(22) = 73.7(6)
O(18) - Dy(2) - O(19) = 100.2(6)
O(18) - Dy(2) - O(20) = 71.8(7)
O(18) - Dy(2) - O(21) = 141.6(6)
O(18) - Dy(2) - O(22) = 145.2(6)
O(19) - Dy(2) - O(20) = 71.4(6)
O(19) - Dy(2) - O(21) = 81.9(6)
O(19) - Dy(2) - O(22) = 74.3(6)
O(20) - Dy(2) - O(21) = 72.7(6)
O(20) - Dy(2) - O(22) = 133.9(6)
O(21) - Dy(2) - O(22) = 72.7(5)

CRYSTAL STRUCTURES

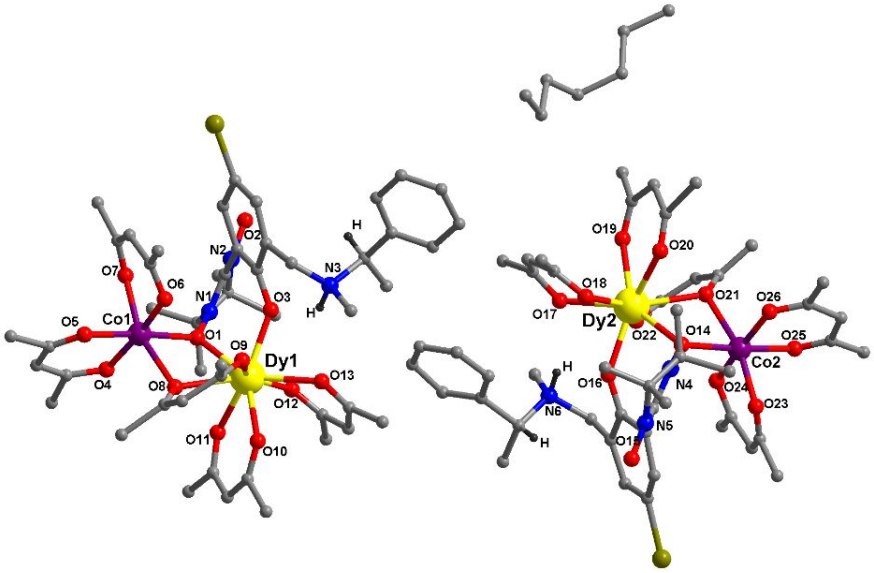

Figure S1. Perspective view of the two crystallographically independent units in crystal **5a.**

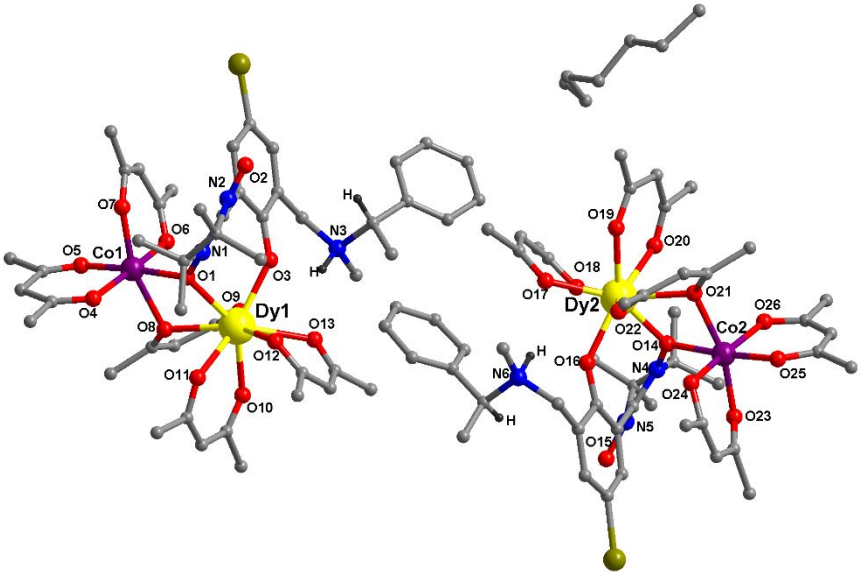

Figure S2. Perspective view of the two crystallographically independent units in crystal **5b.**

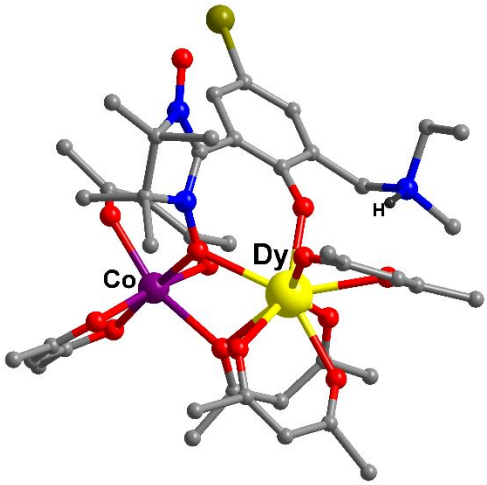

$[CoDy(L^1H)(hfac)_5]\cdot C_6H_{14}$ **1**

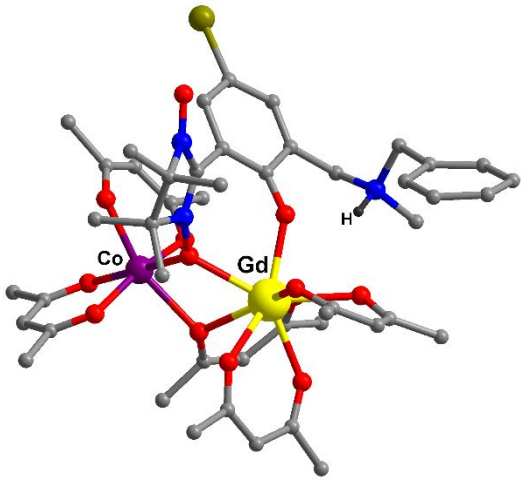

$[CoGd(L^2H)(hfac)_5]$ **2**

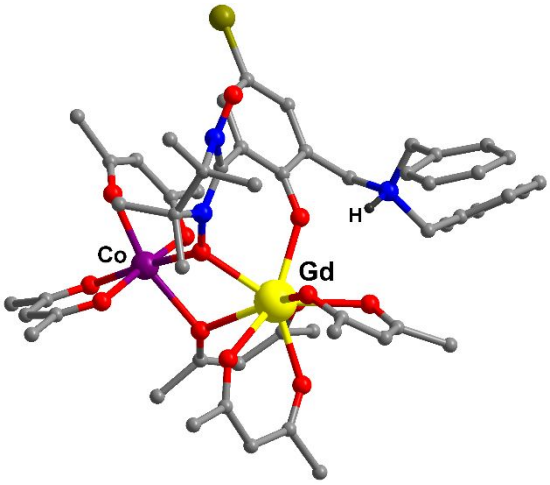

$[CoGd(L^3H)(hfac)_5]$ **3**

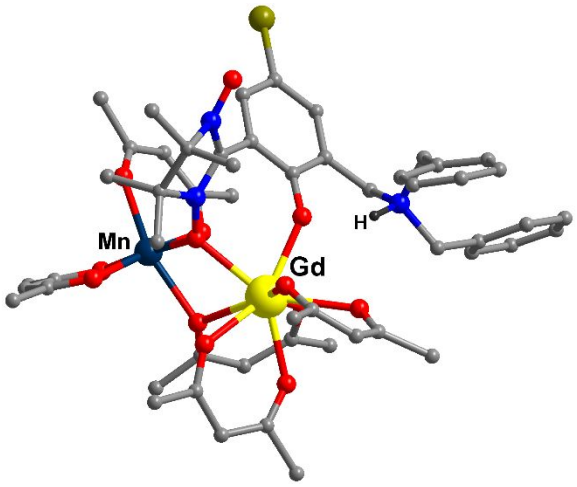

$[MnGd(L^3H)(hfac)_5]$ **4**

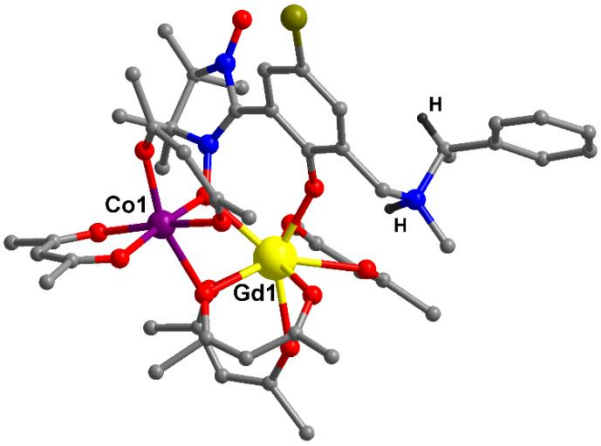

[CoGd(*R*-L^{4}H)(hfac)$_5$]·0.5C$_7$H$_{16}$ **6**

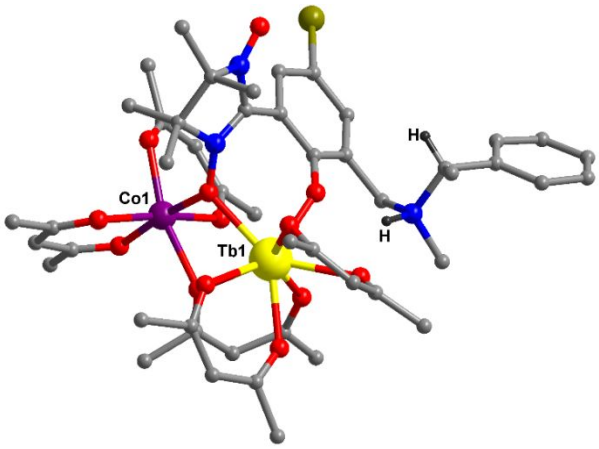

[CoTb(*S*-L^{4}H)(hfac)$_5$]·0.5C$_7$H$_{16}$ **7**

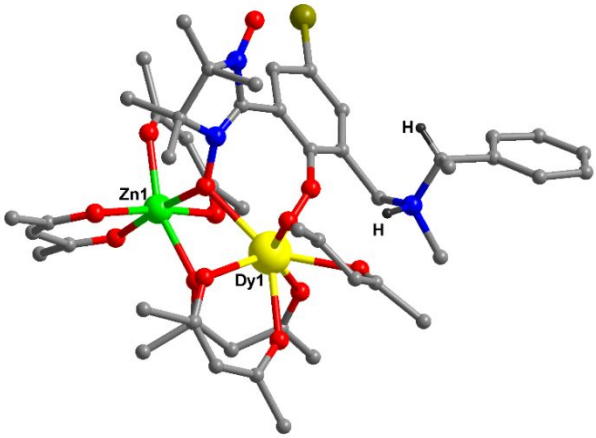

[ZnDy(*S*-L^{4}H)(hfac)$_5$]·0.5C$_7$H$_{16}$ **8**

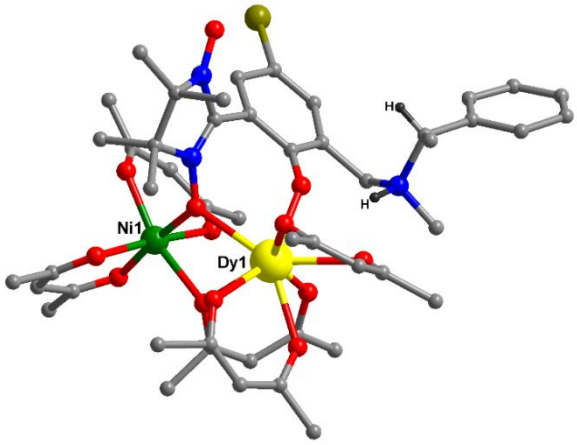

[NiDy(*S*-L^{4}H)(hfac)$_5$]·0.5C$_7$H$_{16}$ **9**

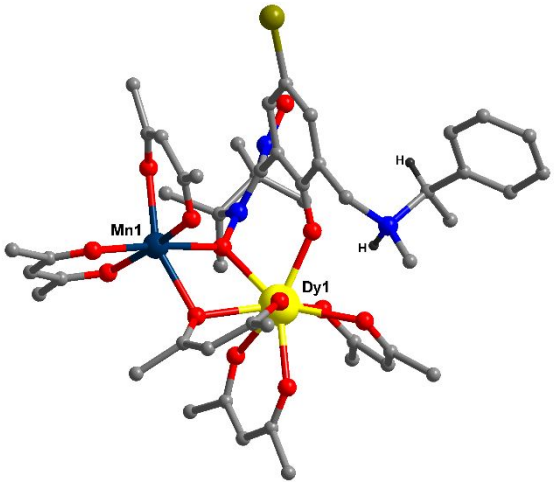

$[MnDy(R\text{-}L^4H)(hfac)_5]\cdot 0.5C_7H_{16}$ **10**

Figure S3. Views of the binuclear complexes in crystals **1**-**4** and **6**-**10**.

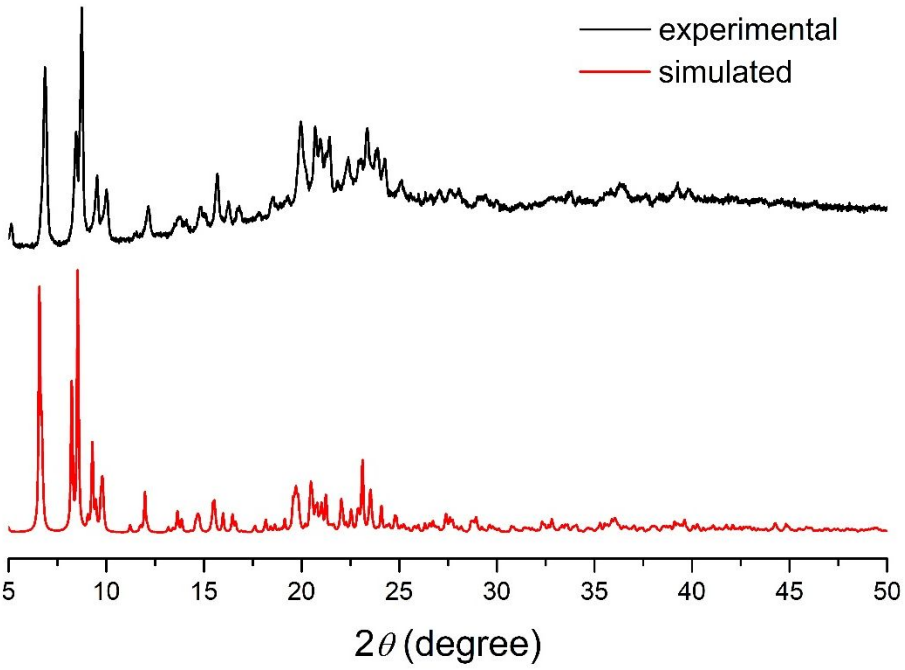

[CoDy(*R*-L^{4}H)(hfac)$_5$]·0.5C$_7$H$_{16}$ **5a**

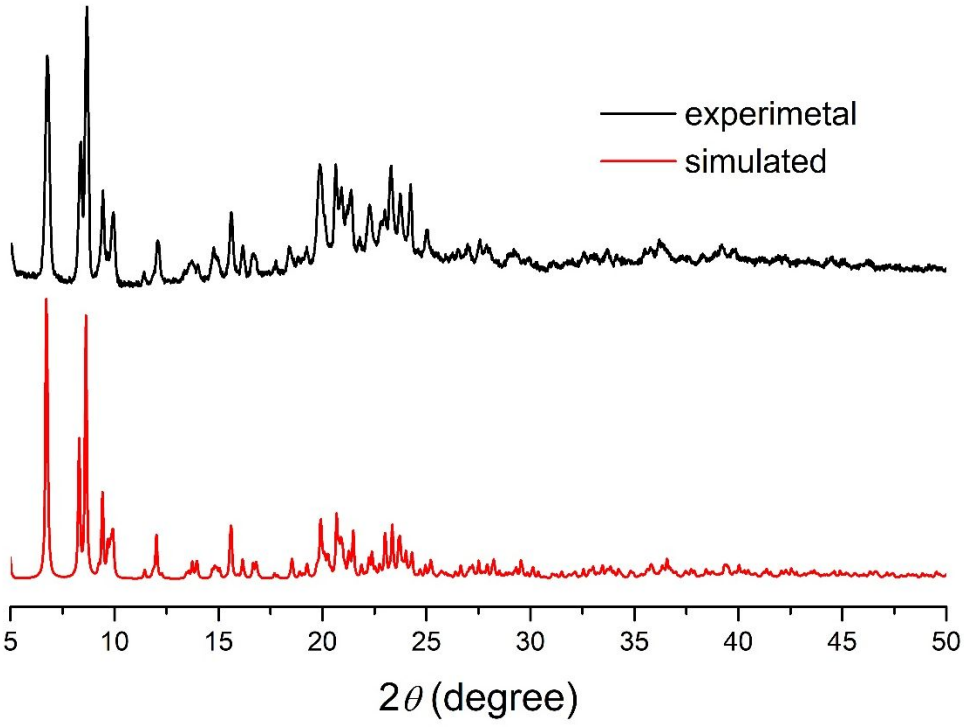

[CoDy(*S*-L^{4}H)(hfac)$_5$]·0.5C$_7$H$_{16}$ **5b**

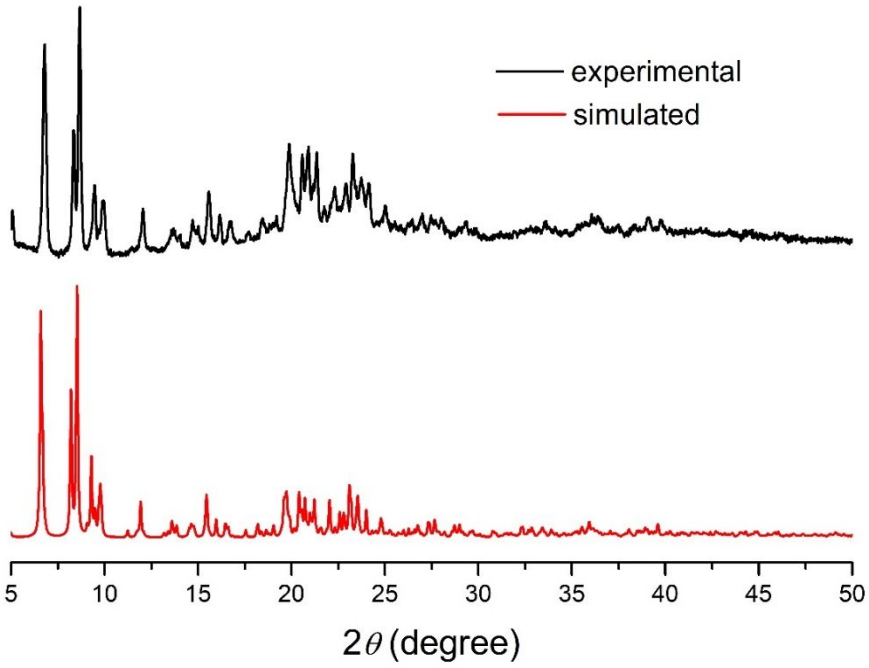

[CoGd(*R*-L^{4}H)(hfac)$_5$]·0.5C$_7$H$_{16}$ **6**

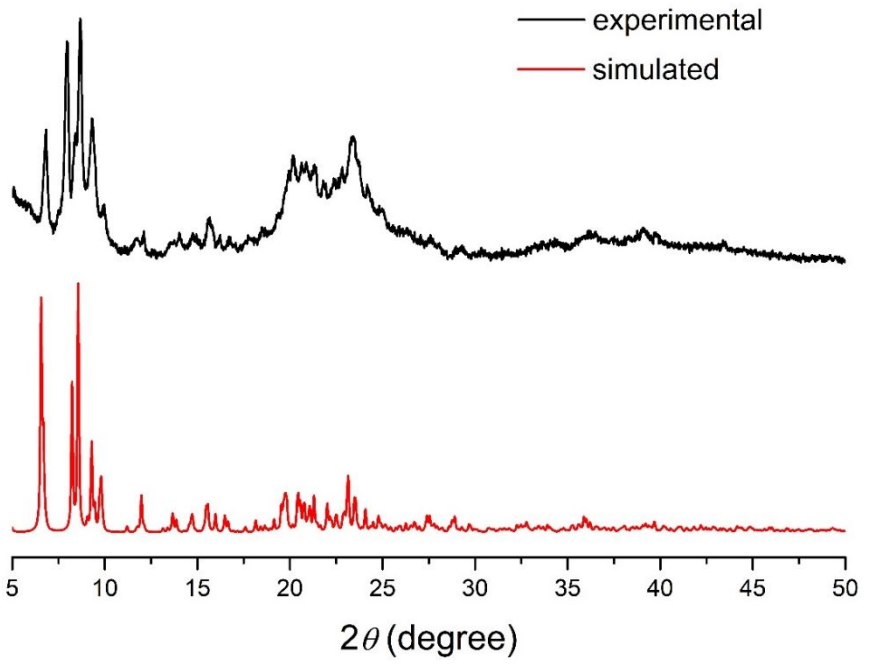

[ZnDy(*S*-L^{4}H)(hfac)$_5$]·0.5C$_7$H$_{16}$ **8**

Figure S4. Simulated and experimental powder X-ray diffractograms for compounds **5a, 5b, 6** and **8.**

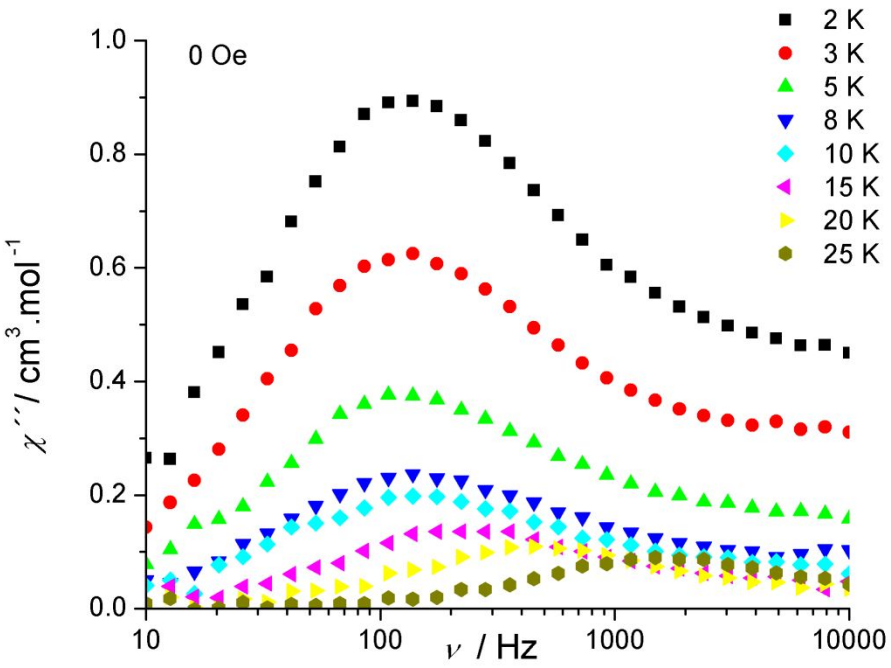

Figure S5. Frequency dependence at different temperatures of the out-of-phase ac magnetic susceptibility χ" of **5a**, under zero applied dc field.

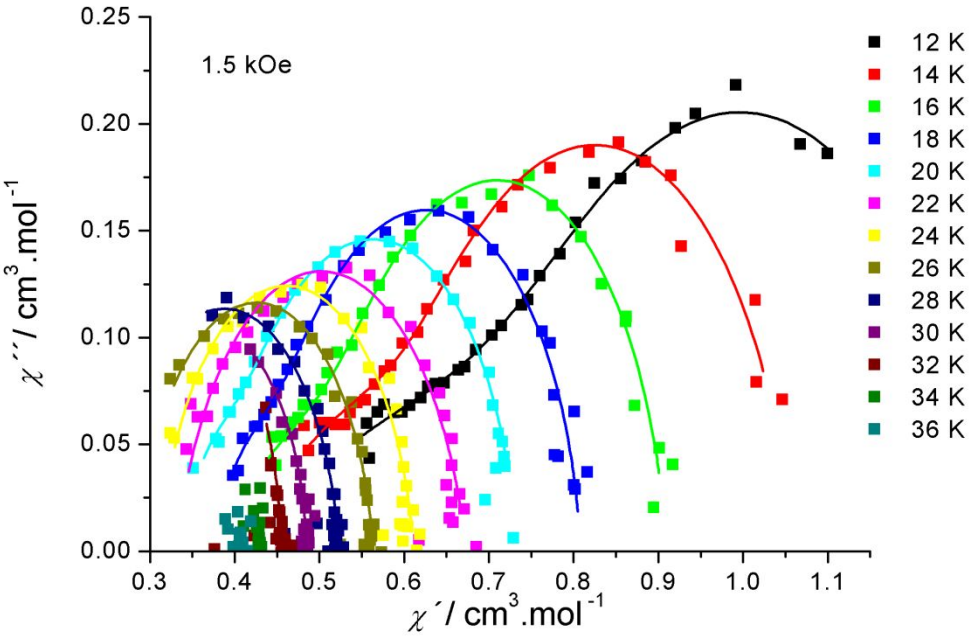

Figure S6. Cole-Cole diagrams at different temperatures for **5a,** under an applied dc field of 1500 Oe.

Table S3: Summary of the parameters for the fit with the modified Debye function for compound $[Co^{II}Dy^{III}(L^4H)(hfac)_5]$.

T (K)	$\chi_{S,tot}(cm^3.mol^{-1})$	$\Delta\chi(cm^3.mol^{-1})$	α	$\tau(s)$
12	0.41	0.37	0.17	8.7 E-3
14	0.42	0.38	0.11	2.8 E-3
16	0.39	0.34	0.10	1.27 E-3
18	0.38	0.34	0.10	6.6 E-4
20	0.34	0.32	0.10	4.1 E-4
22	0.33	0.34	0.16	2.0 E-4
24	0.31	0.30	0.12	1.11 E-4
26	0.29	0.28	0.11	5.1 E-5
28	0.25	0.27	0.12	2.0 E-5
30	0.26	0.22	0.10	1.03 E-5
32	0.20	0.26	0.10	3.8 E-6

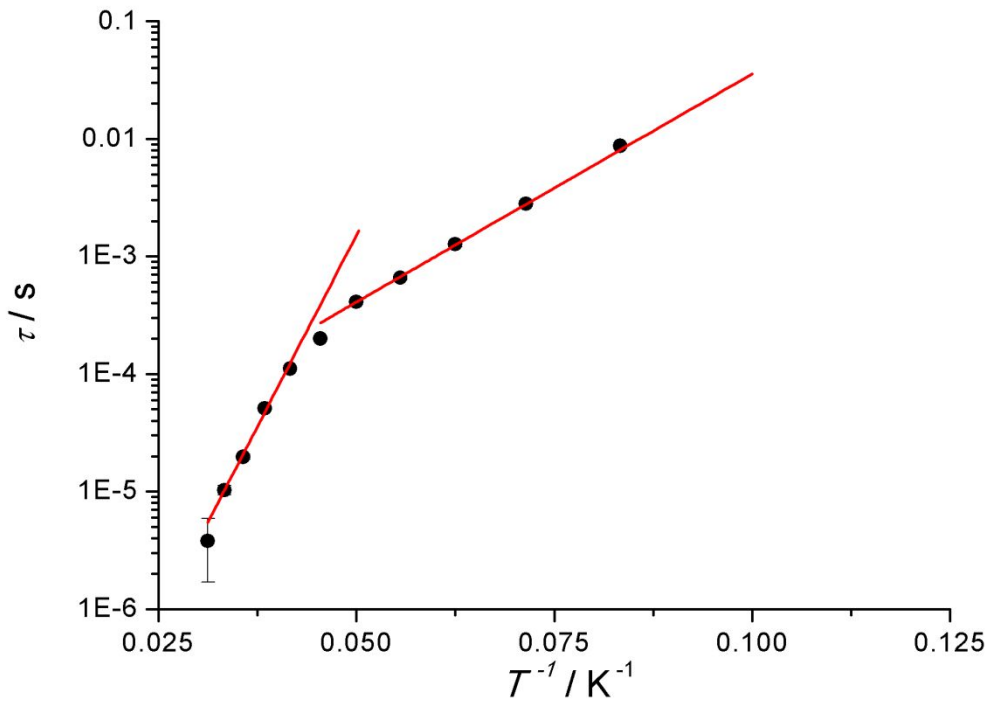

Figure S7. Arrhenius plot from the out-of-phase susceptibility versus frequency at H=1.5 kOe for **5**. The red lines correspond to the best fits from Arrhenius law for the lowest and highest temperatures.

Ab Initio calculations on NNR(+)CoDy chiral compound

Computational details

Table S4. ANO-RCC basis sets[3,4] and contractions employed throughout all the calculations.

Atom	Label	Primitives	Contraction
Dy	VTZP	[25s22p15d11f4g2h]	[8s7p5d3f2g1h]
Co	VTZP	[21s15p10d6f4g2h]	[6s5p3d2f1g]
La	VDZ	[24s21p15d5f3g2h]	[7s6p4d2f]
Zn	VDZ	[21s15p10d6f4g2h]	[5s4p2d1f]
Br	VDZ	[20s17p11d4f2g]	[5s4p2d1f]
N	VTZP	[14s9p4d3f2g]	[4s3p2d1f]
O	VTZP	[14s9p4d3f2g]	[4s3p2d1f]
C	VDZP	[14s9p4d3f2g]	[3s2p1d]
F	VDZ	[14s9p4d3f2g]	[3s2p]
H	VDZ	[8s4p3d1f]	[2s]

Calculations on compounds **5** and **8** were performed with MOLCAS 8.0 quantum chemistry software.[5] For all compounds the geometries resolved by x-ray diffraction were employed. For both compounds calculations were performed on both crystallographic independent molecular units (**A** and **B**) inside the unit cell. In order to reduce the number of primitive functions due to computational limitations, some structural approximations were adopted: i) the x-ray structures were employed replacing -CF_3 groups with CH_3 groups ii) the methyl groups of the NNit moiety were replaced by hydrogens atoms iii) the chiral moiety and the methyl group bonded to the tertiary amine were replaced by hydrogens atoms. The effects on the electronic structure due to the first and the second structural modifications were evaluated in our previous publication,[6] while the third one is also expected not to strongly influence the magnetic properties of the complex due to the distance of the chiral group from the magnetic centers. No further optimization was carried on.

The energy ladder of the electronic states for the dimeric Dy(III) and Co(III) ions obtained by doping the NNit with an extra electron in order to turn it into a diamagnetic ligand have been computed within the CASSCF/CASSI-SO method . The single ion anisotropies of the two metal ions have also been computed on the individual center by diamagnetic substitution on the other

two magnetic centers keeping the radical doped: Zn(II) and La(III) for Co(II) and Dy(III), respectively. The chosen active space for Dy(III) consists of nine electrons in the seven 4f-orbitals of the lanthanide ion: CAS (9,7). Due to hardware limitations, only the 21 sextuplets were computed and included in the following spin-orbit calculation. The chosen active space for Co(II) consists of seven electrons in the seven 3d-orbitals of the metal ion: CAS (7,5). The ten quadruplets and the forty doublets were computed and included in the following spin-orbit calculation. No perturbative method in order to recover part of the dynamical correlation was performed, due to memory limitation.

The g-tensors were computed with the SINGLE_ANISO module.[7] Both metal ions are Kramers' ion due to their odd number of electrons. Their magnetic anisotropy was investigated within the pseudospin framework and their anisotropy axes were calculated with a pseudospin S = 1/2.

To compute the isotropic magnetic coupling between the radical and the metal ions, CASSCF calculations were performed without spin-orbit contribution for the two compounds. In compound **5**, the exchange couplings between the metal ions and the radical were computed singly substituting them in turn by their diamagnetic equivalent (Dy(III) and Co(II) ion or doped state (Rad) (see above). For the Dy(III)-NNit interactions in **5** and **8**, the chosen active space consisted of nine electrons in the seven 4f-orbitals of the lanthanide ion and the unpaired electron in the π* orbital of the O(1)-N(1)-C-N(2)-O(2) system on the radical, CAS (10,8). For the cobalt-radical interaction in DyCoNNit, the active space consisted of the five 3d orbitals and the π* molecular orbital of the Rad, CAS (8,6). Finally, in order to compute the Co-Dy interaction, the GASSCF approach was employed: the radical was not doped but its π* orbitals was considered inactive. Only a maximum of two excitations, GASSCF(2), were allowed from the seven 4f orbitals of the lanthanides to the five 3d orbitals of the Cobalt for computational hardware limitation. Regarding the Dy-rad and Co-rad interactions, calculations were performed converging on both the ferromagnetic and antiferromagnetic states resulting from the coupling of the unpaired electron localized on the radical and the unpaired electrons on the Dysprosium and Cobalt ions: the lowest septuplet and quintuplet states for the interaction Dy-rad; the lowest quintuplet and triplet states for the Co-rad. Regarding the Co-Dy interaction, by means of the previously described GASSCF approach, GASSCF(2), it was possible to converge to the lowest decuplet and octuplet states in energy.

The values of the exchange coupling constants were computed within the Heisenberg model, therefore using the real *S* values of each magnetic species involved, i.e. ½, 3/2, 5/2, for Rad, Co(III), and Dy(III), respectively:

$$J_{Heis} = \frac{-(E_{HS} - E_{LS})}{S_{HS}}$$

E_{HS} and E_{LS} are the energy of the High Spin (ferro) and Low Spin (antiferro) configurations, respectively, and S_{HS} is the spin quantum number of the HS configuration.

The χT curves were simulated by means of the POLY_ANISO software with the Lines' model. In the Lines model the Heisenberg isotropic exchange interaction is firstly computed between isotropic spin multiplets (S = 5/2 for Dy and S = 3/2 for Co) and then projected on the basis of the previously computed spin-orbit states. In our models, for compound **8** only the exchange coupling interaction between the lanthanide and the coordinated isotropic S = ½ of the radical was considered, while for compound **5** all the three exchange coupling interactions between the lanthanide, the cobalt ion, and the radical were considered, since none of the three can be neglected as suggested by ab initio calculations. The exchange interactions have been computed considering only the six lowest states in energy of the lanthanide ion, the four lowest ones of the Cobalt ion and the isotropic doublet of the radical. In order to reproduce the high temperature data also the single ion crystal field splitting for the two metal ions was included in the model. In this Hamiltonian, the only parameter present is the exchange coupling constant J_{Lines} since all the information about crystal field splitting and magnetic anisotropy are computed *ab initio*. J_{Heis} have been successfully used as guess values for the J_{Lines}.

Single Ions' properties

Table S5. Values of the main magnetic axes of the ground Kramers' doublet for Dy and Co in $[Co^{II}Dy^{III}(R\text{-}L^4H)(hfac)_5]$ (**5a**), and their orientations in the crystal frame, mapped within the pseudospin approach.

5a$_{(R\Delta\Delta)}$		**Value**	**a**	**b'**	**c***
	$\mathbf{g_x}$	0.0058	-0.882951	0.463619	-0.073857
Dy	$\mathbf{g_y}$	0.0087	-0.235528	-0.573546	-0.784584
	$\mathbf{g_z}$	19.7340	-0.406109	-0.675354	0.615608
	$\mathbf{g_x}$	1.8196	0.633123	0.737419	-0.235305
Co	$\mathbf{g_y}$	2.8465	-0.580585	0.653458	0.485710
	$\mathbf{g_z}$	7.7689	0.511934	-0.170900	0.841853

5a$_{(S\Delta\Delta)}$		**Value**	**a**	**b'**	**c***
	$\mathbf{g_x}$	0.02332	0.917023	-0.247044	0.313111
Dy	$\mathbf{g_y}$	0.05894	-0.039278	0.725308	0.687303
	$\mathbf{g_z}$	19.4214	-0.396896	-0.642571	0.655421
	$\mathbf{g_x}$	2.3894	0.707441	0.600145	-0.373300
Co	$\mathbf{g_y}$	3.5255	-0.084837	0.596464	0.798144
	$\mathbf{g_z}$	6.8794	0.701662	-0.532970	0.472878

Table S6. Computed energy levels at CASSCF/RASSI-SO level for both ions in compound **5a** and **8a**.

	5a				**8a**	
Energy level (cm^{-1})	**Dy ($5a_{(R\Delta\Lambda)}$)**	**Dy ($5a_{(S\Lambda\Delta)}$)**	**Co ($5a_{(R\Delta\Lambda)}$)**	**Co ($5a_{(S\Lambda\Delta)}$)**	**Dy ($5a_{(R\Delta\Lambda)}$)**	**Dy ($5a_{(S\Lambda\Delta)}$)**
1	0.000	0.000	0.000	0.000	0.000	0.000
2	0.000	0.000	0.000	0.000	0.000	0.000
3	197.931	108.129	217.284	220.897	205.698	101.004
4	197.931	108.129	217.284	220.897	205.698	101.004
5	301.365	131.324	684.333	583.357	304.036	132.247
6	301.365	131.324	684.333	583.357	304.036	132.247
7	348.618	176.588	984.865	959.938	360.919	179.947
8	348.618	176.588	984.865	959.938	360.919	179.947
9	378.475	202.590	1464.201	1188.621	412.534	211.288
10	378.475	202.590	1464.201	1188.621	412.534	211.288
11	432.509	227.042	1542.530	1326.501	446.820	257.176
12	432.509	227.042	1542.530	1326.501	446.820	257.176
13	479.770	303.229	6325.307	6581.984	543.635	380.148
14	479.770	303.229	6325.307	6581.984	543.635	380.148
15	598.068	443.356	6405.829	6651.357	608.255	467.173
16	598.068	443.356	6405.829	6651.357	608.255	467.173
17	3095.088	3059.201	7341.103	7317.638	3100.459	3057.533
18	3095.088	3059.201	7341.103	7317.638	3100.459	3057.533
19	3208.104	3108.965	7395.971	7356.012	3216.690	3092.346
20	3208.104	3108.965	7395.971	7356.012	3216.690	3092.346
21	3298.899	3133.465	7698.528	7571.395	3319.518	3136.437
22	3298.899	3133.465	7698.528	7571.395	3319.518	3136.437
23	3342.445	3172.703	7832.410	7694.136	3359.576	3184.592
24	3342.445	3172.703	7832.410	7694.136	3359.576	3184.592
25	3380.202	3204.507	14360.464	14624.165	3389.627	3240.585
26	3380.202	3204.507	14360.464	14624.165	3389.627	3240.585
27	3400.958	3223.529	14658.924	14793.145	3427.933	3277.236
28	3400.958	3223.529	14658.924	14793.145	3427.933	3277.236
29	3460.149	3283.858	14662.302	14796.955	3501.674	3316.444
30	3460.149	3283.858	14662.302	14796.955	3501.674	3316.444
31	5733.824	5655.743	16980.704	16150.127	5743.732	5654.085
32	5733.824	5655.743	16980.704	16150.127	5743.732	5654.085
33	5807.920	5683.764	19862.929	20055.984	5818.005	5679.084
34	5807.920	5683.764	19862.929	20055.984	5818.005	5679.084
35	5870.164	5732.173	20002.941	20226.597	5894.922	5745.690

36	5870.164	5732.173	20002.941	20226.597	5894.922	5745.690
37	5916.617	5764.787	20347.966	20557.830	5928.915	5788.111
38	5916.617	5764.787	20347.966	20557.830	5928.915	5788.111
39	5944.464	5789.462	21149.158	20941.560	5961.344	5817.120
40	5944.464	5789.462	21149.158	20941.560	5961.344	5817.120
41	6029.330	5822.561	21687.856	21279.539	6067.798	5865.869
42	6029.330	5822.561	21687.856	21279.539	6067.798	5865.869

The Dy ion shows a pronounced easy axis anisotropy, while the situation for Co(II) is intermediate between easy axis and easy plane. Indeed, if we go beyond the pseudospin approach, and we map the Co(II) anisotropy within the following zero field splitting hamiltonian,

$$H_{zfs} = D\cdot\left[S_z^2 - S\cdot\frac{S+1}{3}\right] + E\cdot\left[S_x^2 - S_y^2\right]$$

where the effective spin S=3/2 for Co(II) is employed, the obtained parameters are reported in Table S7. As we can observe, the value for E is near the limit of D/3, indicating a strong rhombic contribution, i.e. large deviation from axiality.

Table S7. Computed Zero Field Splitting (in cm^{-1}) parameters for Co(II) ion in compound **5a**.

	D	**E**
5a$_{(R\Delta\Lambda)}$	95.4821	-29.9239
5a$_{(S\Lambda\Delta)}$	103.5634	-22.1624

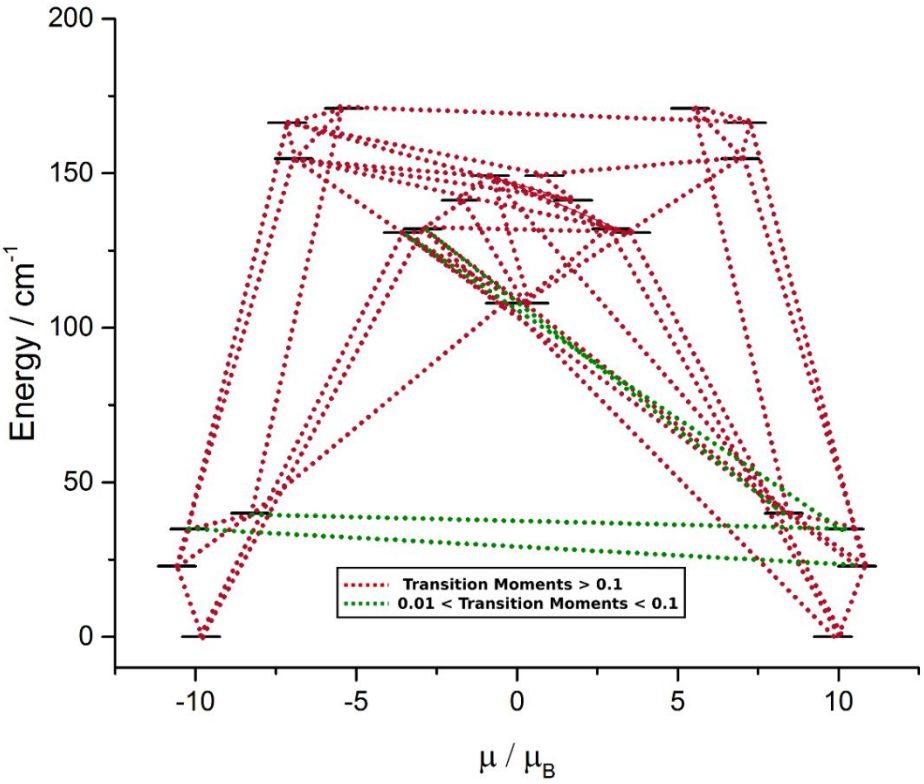

Figure S8. Exchange Kramers'doublets up to 200 cm^{-1} and transition magnetic moments in $[Co^{II}Dy^{III}(R\text{-}L^4H)(hfac)_5]$ unit $\mathbf{5a}_{(SAA)}$, computed within the Lines' model.

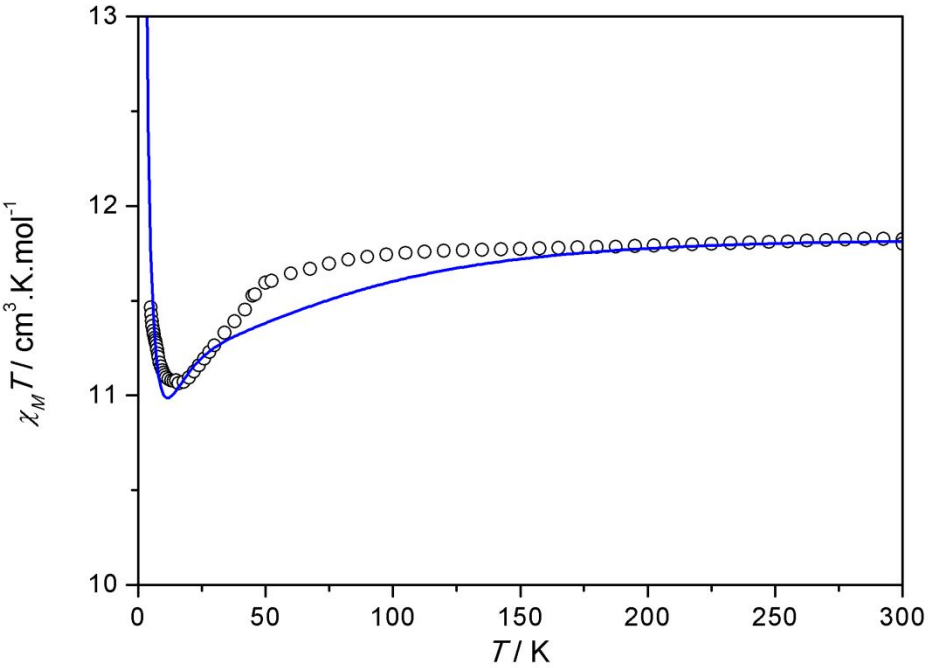

Figure S9. Temperature dependence of $\chi_M T$ for $[Co^{II}Gd^{III}(L^4H)(hfac)_5]$ **6**. The blue line represents the simulation with the same set of parameters employed for **5** (vide text).

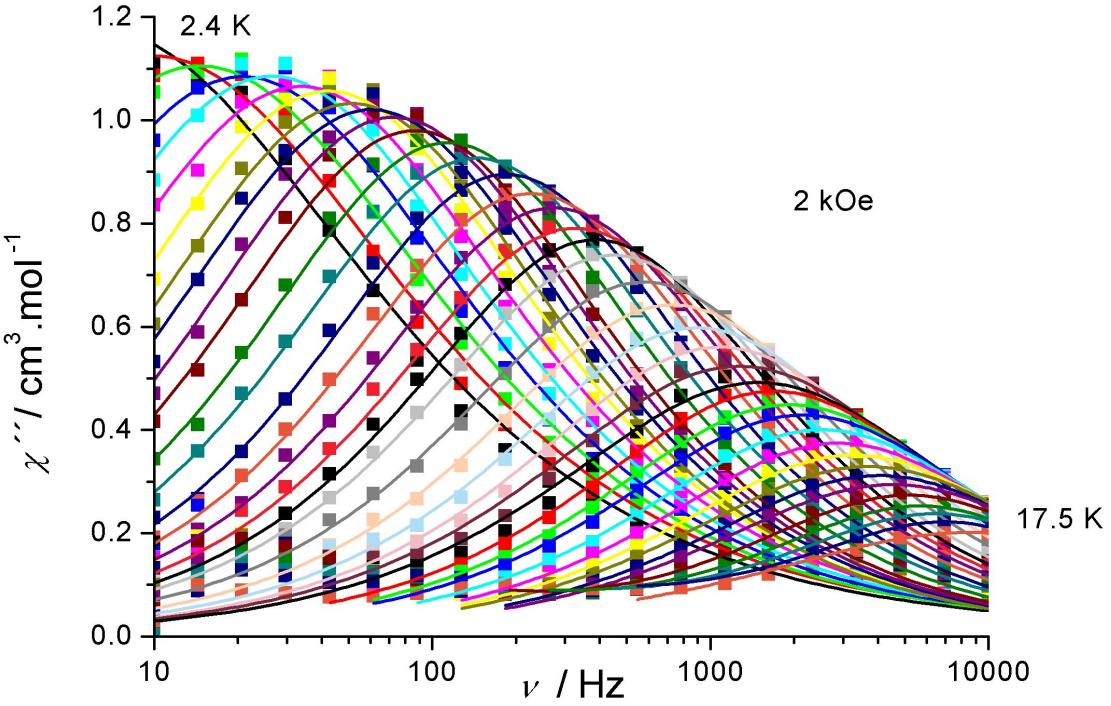

Figure S10. Frequency dependence at different temperatures of the out-of-phase ac magnetic susceptibility χ" of **8**, under an applied dc field of 2000 Oe.

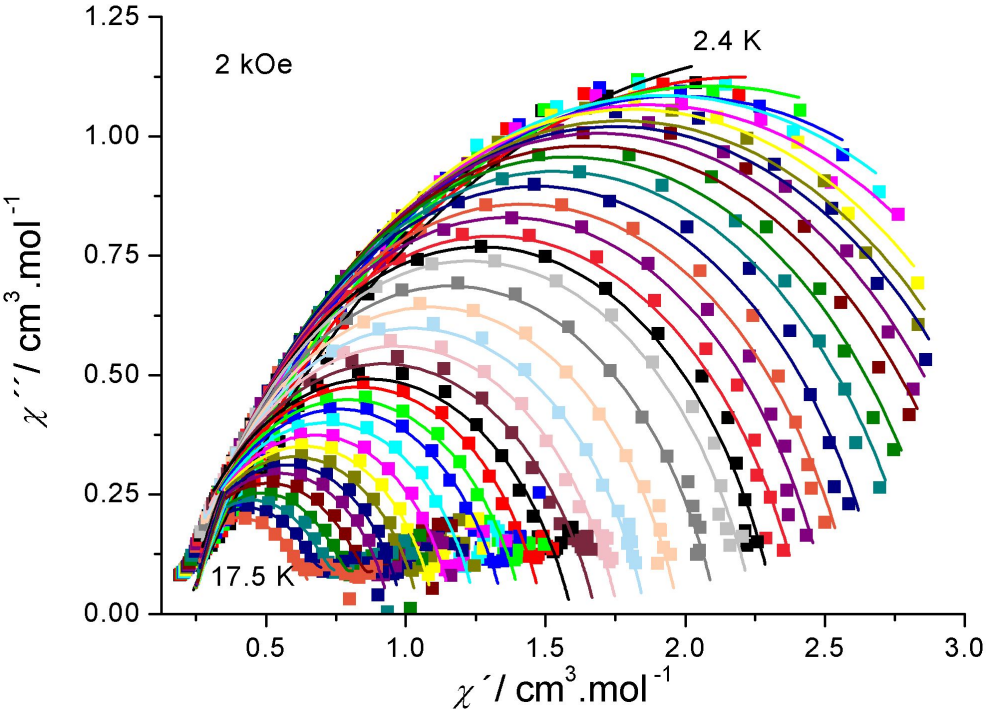

Figure S11. Cole-Cole diagrams at different temperatures for **8,** under an applied dc field of 2000 Oe.

Table S8: Summary of the parameters for the fit with the modified Debye function for compound $[Zn^{II}Dy^{III}(L^4H)(hfac)_5]$.

T (K)	$\chi_{S,tot}(cm^3.mol^{-1})$	$\Delta\chi(cm^3.mol^{-1})$	α	$\tau(s)$
2.4	0.21	4.4	0.38	2.5 E-2
2.5	0.22	3.96	0.35	15.8 E-3
2.6	0.23	3.73	0.33	10.9 E-3
2.7	0.23	3.48	0.3	7.6 E-3
2.8	0.24	3.37	0.28	6.0 E-3
2.9	0.23	3.28	0.27	4.7 E-3
3.0	0.24	3.15	0.26	3.7 E-3
3.1	0.23	3.1	0.25	3.1 E-3
3.2	0.22	3.04	0.25	2.63 E-3
3.3	0.23	2.94	0.24	2.19 E-3
3.4	0.23	2.83	0.23	1.84 E-3
3.6	0.23	2.72	0.22	1.40 E-3
3.8	0.22	2.63	0.22	1.10 E-3
4.0	0.23	2.49	0.21	8.6 E-4
4.2	0.22	2.39	0.21	7.0 E-4
4.4	0.22	2.30	0.20	5.8 E-4
4.6	0.21	2.18	0.20	4.9 E-4
4.8	0.22	2.11	0.20	4.1 E-4
5.0	0.21	2.04	0.20	3.56 E-4
5.4	0.20	1.91	0.21	2.75 E-4
5.8	0.20	1.78	0.20	2.18 E-4
6.2	0.19	1.67	0.21	1.77 E-4
6.6	0.18	1.58	0.22	1.47 E-4
7.0	0.16	1.53	0.23	1.25 E-4
7.4	0.14	1.45	0.24	1.07 E-4
7.8	0.17	1.32	0.21	9.4 E-5
8.2	0.17	1.24	0.20	8.3 E-5

8.6	0.17	1.18	0.20	7.4 E-5
9.2	0.17	1.08	0.19	6.3 E-5
9.8	0.18	0.99	0.18	5.5 E-5
10.4	0.17	0.94	0.18	4.9 E-5
11.0	0.15	0.90	0.19	4.3 E-5
11.6	0.16	0.83	0.18	3.9 E-5
12.2	0.15	0.80	0.19	3.5 E-5
13.0	0.14	0.73	0.16	3.0 E-5
14.0	0.16	0.63	0.13	2.7 E-5
15.0	0.16	0.57	0.11	2.4 E-5
16.0	0.18	0.49	0.10	2.2 E-5
17.5	0.12	0.56	0.24	1.9 E-5

Table S9. Computed *ab initio* and simulated (POLY_ANISO) $J_{Dy\text{-}Rad}$ exchange coupling constants (in cm^{-1}) for compound **8a.**

	8a$_{(R\Delta\Delta)}$	**8a**$_{(S\Delta\Delta)}$
Computed	0.70524	1.1632
Simulated	4.4	

References

(1) Crane, J. D.; Fenton, D. E.; Latour, J. M.; Smith, A. J. Unsymmetric dicopper(II) complexes of dinucleating ligands bearing chemically distinct co-ordination environments. *J. Chem. Soc. Dalt. Trans.* **1991**, *11*, 2979.

(2) Farrugia, L. J.; WinGX. *J. Appl. Cryst.* **2012**, *45*, 849-854.

(3) Veryazov, V.; Widmark, P.-O.; Roos, B. O. Relativistic atomic natural orbital type basis sets for the alkaline and alkaline-earth atoms applied to the ground-state potentials for the corresponding dimers. *Theor. Chem. Accounts Theory, Comput. Model. (Theoretica Chim. Acta)* **2004**, *111*, 345–351.

(4) Roos, B. O.; Lindh, R.; Malmqvist, P.-A.; Veryazov, V.; Widmark, P.-O.; Borin, A. C. New relativistic atomic natural orbital basis sets for lanthanide atoms with applications to the Ce diatom and LuF3. *J. Phys. Chem. A* **2008**, *112*, 11431-11435.

(5) Aquilante, F.; Autschbach, J.; Carlson, R. K.; Chibotaru, L. F.; Delcey, M. G.; De Vico, L.; Fdez. Galván, I.; Ferré, N.; Frutos, L. M.; Gagliardi, L.; et al. Molcas 8: New capabilities for multiconfigurational quantum chemical calculations across the periodic table. *J. Comput. Chem.* **2016**, *37*, 506–541.

(6) Patrascu, A. A.; Calancea, S.; Briganti, M.; Soriano, S.; Madalan, A. M.; Allão Cassaro, R. A.; Caneschi, A.; Totti, F.; Vaz, M. G. F.; Andruh, M. A chimeric design of heterospin 2p–3d, 2p–4f, and 2p–3d–4f complexes using a novel family of paramagnetic dissymmetric compartmental ligands. *Chem. Commun*. **2017**, *53*, 6504-6507.

(7) Chibotaru, L. F.; Ungur, L. Ab Initio calculation of anisotropic magnetic properties of complexes. I. Unique definition of pseudospin Hamiltonians and their derivation. *J. Chem. Phys.* **2012**, *137*, 064112.